Journal of Colloid and Interface Science 662 (2024) 471–478

Contents lists available at ScienceDirect

Journal of Colloid And Interface Science

journal homepage: www.elsevier.com/locate/jcis

Regular Article

# Pickering stabilization mechanism revealed through direct imaging of particles with tuneable contact angle in a phase-separated binary solvent

Fu Zhen Zhou [a,b,c], Piet J.M. Swinkels [b], Shou Wei Yin [c,d], Krassimir P. Velikov [b,e,f], Peter Schall [b,*]

[a] College of Food Science, Fujian Agriculture and Forestry University, Fuzhou, PR China
[b] Institute of Physics, University of Amsterdam, Amsterdam, The Netherlands
[c] Research and Development Center of Food Proteins, Guangdong Province Key Laboratory for Green Processing of Natural Products and Product Safety, Department of Food Science and Technology, South China University of Technology, Guangzhou, 51640, PR China
[d] Sino-Singapore International Joint Research Institute, Guangzhou 510640, PR China
[e] Unilever Innovation Centre Wageningen, Bronland 14, 6708 WH, Wageningen, The Netherlands
[f] Soft Condensed Matter, Debye Institute for Nanomaterials Science, Utrecht University, Princetonplein 5, 3584 CC, Utrecht, The Netherlands

## GRAPHICAL ABSTRACT

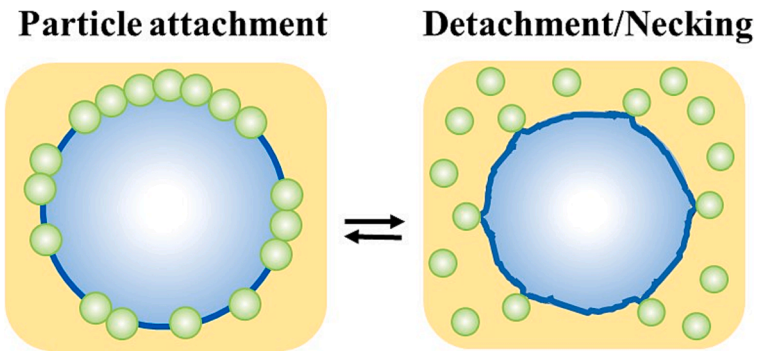


## ARTICLE INFO

*Keywords:*
Pickering emulsion
Colloids
Binary liquid
Capillary interactions
Interfacial energy and contact angle

## ABSTRACT

Pickering emulsions have attracted increasing attention from multiple fields, including food, cosmetics, healthcare, pharmaceutical, and agriculture. Their stability relies on the presence of colloidal particles instead of surfactant at the droplet interface, providing steric stabilization. Here, we demonstrate the microscopic attachment and detachment of particles with tunable contact angle at the interface underlying the Pickering emulsion stability. We vary the interfacial tension continuously by varying the temperature offset of a phase-separated binary liquid from its critical point, and employ confocal microscopy to directly observe the particles at the interface to determine their coverage and contact angle as a function of the varying interfacial tension. When the interfacial tension decreases upon approaching the binary liquid's critical point, the contact angle and detachment energy ($\Delta E$) drop, and the particles move out of the interface. Microscopic imaging suggests necking and capillary interactions lead to clustering of the particles, before they eventually desorb from the interface. Macroscopic measurements show that concomitantly, coalescence takes place, and the emulsion loses its stability. These results reveal the interplay of interfacial energies, contact angle and surface coverage that underlies

* Corresponding author.

https://doi.org/10.1016/j.jcis.2024.02.070
Received 31 October 2023; Received in revised form 18 January 2024; Accepted 6 February 2024
Available online 10 February 2024

the Pickering emulsion stability, opening up ways to manipulate and design the stability through the microscopic behavior of the adsorbed particles.

## 1. Introduction

Emulsions are very common in daily life, and exist in many industries such as food, cosmetics, healthcare, pharmaceutical and agricultural etc. While it is well known that oil and water are immersible with each other, and the emulsified system is thermodynamically unstable [1], the use of stabilizer is necessary to restrain the coalescence of droplets to obtain a stable emulsion. One of the most popular stabilizers is surfactant with a hydrophilic head and a hydrophobic tail [2], for non-polar solvent - in - polar solvent (e.g. oil-in-water) emulsions, and hydrophobic head and a hydrophilic tail for inverse emulsions (e.g. water-in-oil emulsions). Another way of stabilizing the emulsion is by using surface-active particles; the corresponding emulsions are known as Pickering emulsions [3]. Once particles anchor at the oil–water interface, they are usually considered irreversibly adsorbed, because the thermal energy $k_BT$ is much smaller than the energy of detachment. The detachment energy $\Delta E$ can be related to the interfacial tension $\gamma_{ow}$ of the liquid phases via the contact angle $\theta$ of the particle at the interface following [4]:

$$\Delta E = \pi R^2 \gamma_{ow}(1 - |cos\theta|)^2 \ , \quad (1)$$

where $R$ is the radius of the particles. Since this kind of irreversible particle attachment forms a steric barrier at the interface, it can be more effective than surfactant stabilization; therefore, Pickering emulsions are considered to have high stability to coalescence [5–7], low allergy risk [8], and can be widely applied in food, biomedical and material fields [9]. In the past decades, there has been growing effort on Pickering emulsions, with more and more particles being tested and applied as Pickering stabilizers. Those particles include inorganic particles [10] (e.g. silica based), and biobased particles [11] (e.g. cellulose-based [12,13]), including food-grade particles [14] (e.g. starch-based [15], protein particles [16–18]) among others. As the physicochemical properties of the emulsions are crucially dependent on the particle adsorption at the interface, insight into the microscopic process of particle attachment and detachment and its dependence on the interface properties is vital for understanding the Pickering stabilization mechanism. Direct visualization through microscopic techniques such as optical microscopy is a convenient method for investigating the dynamic particle behavior at the interface. Using confocal microscopy, French *et al.,* observed silica particle exchange between droplets in a Pickering

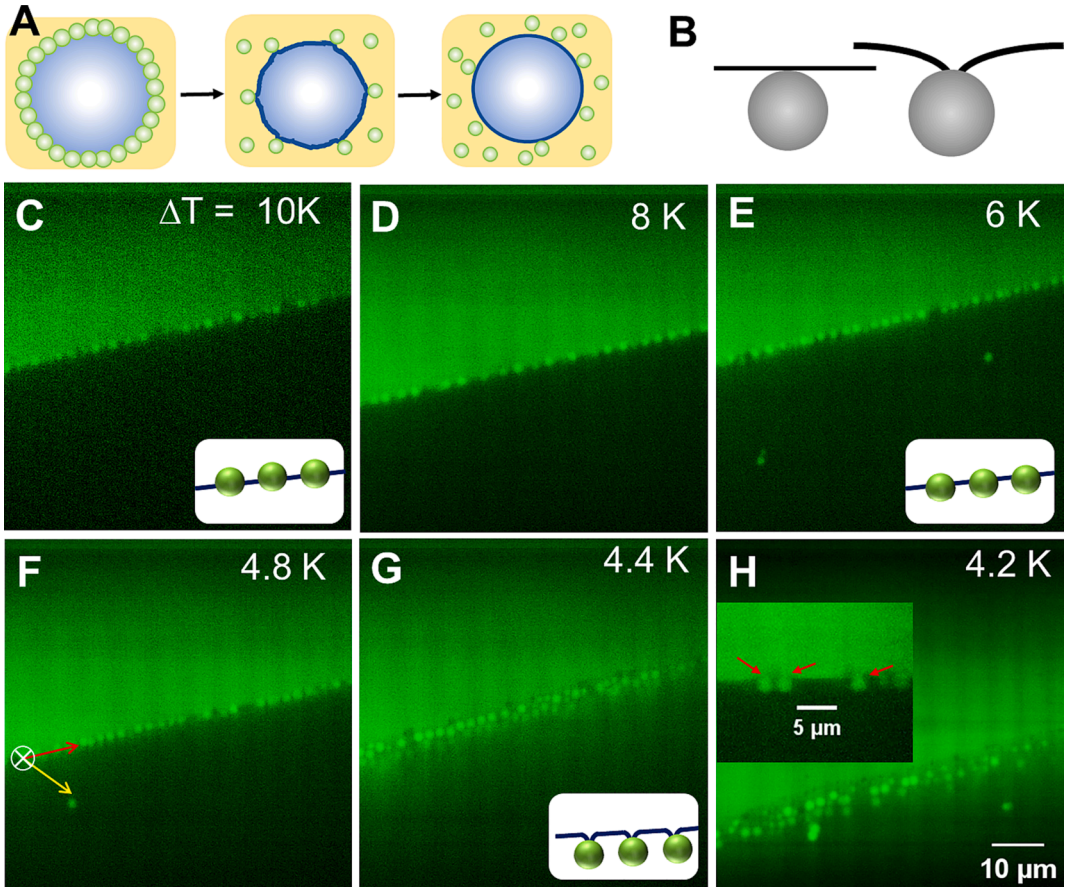


**Fig. 1. Observation of particle detachment.** (A) Illustration of particles detaching from the interface of an emulsion droplet. Capillary bridges are formed upon particle detachment (center image). (B) Illustration of necking, i.e. the formation of a capillary bridge between a particle and the interface. (C—H) Confocal microscope images showing cross sections through a particle-laden interface between lutidine-rich (top, bright) and water-rich (bottom, dark) phases of a phase-separated binary liquid at various temperature offsets $\Delta T$ from the liquid critical point $T_c$: 10 K (C), 8 K (D), 6 K (E), 4.8 K (F), 4.4 K (G), and 4.2 K (H).The particles are visible as bright spots. Upon approaching $T_c$, the particles that are initially centered at the interface move into the water-rich phase. Inset in H highlights the necking of particles at the interface (red arrows) observed at small $\Delta T$. Directions of interface, particle detachment and gravity are indicated in (F) by red, yellow and white arrows, respectively, the latter going into the image plane. (For interpretation of the references to colour in this figure legend, the reader is referred to the web version of this article.)

emulsion [19], while combing optical and atomic force microscopy (AFM), Chai *et al.,* [20] revealed that early attachment of carboxylated silica nanoparticles (NPs) followed a diffusion-controlled process, in which the local areal density of NPs could affect the packed structure. Obviously, interfacial behavior of particles plays an important role in the surface architecture of droplets.

The interfacial tension γ determining the particle absorption via Eq. (1) is usually fixed, given by the properties of the two immiscible liquids. Binary liquids, which exhibit a miscibility gap below or above their critical point, allow continuous variation of the interfacial tension of the phase-separated liquid, permitting direct observation of the Pickering emulsion mechanism as a function of the interfacial tension.

Here, we investigate in detail the attachment and detachment of particles in a Pickering system upon changes in interfacial tension, and link it to the stability of the emulsion. We study Pickering emulsions in a phase-separated binary liquid, in which the interfacial tension and particle solvent affinity change reversibly with temperature, allowing us to vary the particle contact angle and to directly observe the particle desorption from the interface. In our binary liquid below $T_c$, the binary liquid components are miscible, forming a homogenous liquid, while above $T_c$, the binary liquid has a miscibility gap and phase separates. Previous work has focused on the spinodal phase-separation process, in which colloidal particles were used to stabilize the bicontinuous interface formed via spinodal liquid de-mixing, creating a bicontinuous Pickering emulsions known as bijel [21–23] and temperature triggered phase inversion in regular Pickering emulsions [24,25]. We investigate the role of microscopic attachment and detachment of particles at the interface and the underlying effect on emulsion stability. We focus on the deep quench, where upon phase-separation, the system initially forms an emulsion, whose surface tension is set by the temperature offset $\Delta T = T\text{-}T_c$ to the critical temperature $T_c$. Approaching $T_c$ along the critical concentration ($c_c$) decreases the composition difference between the two phases and lowers the surface tension, until at $T_c$, the compositions match and the interface tension between the two phases vanishes. We exploit this tunability to directly observe the particle desorption from the interface at decreasing surface tension, as illustrated in Fig. 1A, and to elucidate its relation to the emulsion stability. By tracking the particle positions at the interface, we measure their contact angle, and connect it to the interface tensions of liquid and solid components and the particle surface coverage. This allows us in detail to follow how the particles leave the interface as a function of the diminishing interface tension and contact angle. We relate this microscopic desorption behavior to the macroscopic emulsion stability. These direct microscopic observations elucidate the interplay of interfacial tension, solvent affinity and thermal fluctuations that underlies the particle desorption process and related Pickering emulsion stability.

## 2. Materials and methods

### 2.1. Preparation of particle dispersion in lutidine-water mixture

We use poly (2,2,2-trifluoroethyl methacrylate) particles synthesized according to the method by Kodger et al., [26], with a radius of $R = 1.06$ μm and polydispersity of 0.09. Following the method reported by Swinkels et al., [27], these particles are suspended in a binary mixture of lutidine (≥99.0 %, Sigma-Aldrich) and water, prepared at the critical concentration of $c_c = 28$ wt% lutidine. The particles are stable and do not swell in the lutidine solvent; furthermore, their low refractive index is reasonably close to that of the lutidine-water mixture, allowing imaging of the particles in the bulk without too much scattering. The particle volume fraction is $\phi = 0.002$ %; experiments conducted at different particle volume fraction show that the particle detachment behavior, within reasonable limits of low $\phi$, does not depend on $\phi$, see Supplementary Data 1A. The mixture phase separates above the critical temperature $T_c = 33.6$ °C, in agreement with previously published values [24,27]. We add a small amount of fluorescent dye (Rhodamine), which dissolves mostly in the (more apolar) lutidine-rich phase, allowing distinction of lutidine-rich and (more polar) water-rich phases as mildly bright and dark areas, respectively, under fluorescent imaging. Similarly, the particles are fluorescently died, making them visible as bright spots. The sample of binary liquid with colloidal particles (0.002 %, v/v) is loaded into a glass capillary (Vitrotubes, Rectangle Boro Tubing 0.10 × 1.00 mm) and sealed with teflon grease (Krytox GPL-205).

### 2.2. Sample characterization

To induce phase separation in the binary liquid and form a stable emulsion, we quench the sample from the one-phase regime below $T_c$ to the two-phase regime above $T_c$ using a well-controlled microscope temperature stage. We quench to $\Delta T = 10$ K above $T_c$, during which the sample spontaneously forms an emulsion of lutidine-rich in a lutidine-poor phase upon crossing $T_c$. During the initial emulsification, the particles attach immediately to the interface; the initially formed emulsion shortly after phase separation is shown in Supplementary Figure 4. The lutidine-rich emulsion phase is confirmed by the fluorescent images showing bright emulsion droplets on a dark background due to the preference of rhodamine for the lutidine-rich phase, see Supplementary Figure 5. After the quench, we wait one hour for equilibration. Confocal microscopy (Zeiss LSM 5 Live laser scanning confocal microscope) is used to image the particles at the liquid–liquid interface roughly 20 μm above the capillary wall. To observe the particle desorption from the interface, we then lower the temperature in steps of 1 K or smaller towards $T_c$, while waiting at least one hour for equilibration at each temperature. After equilibration, we acquire images from 10 fields of view along the interface to capture more than 200 particles at the interface. We then use particle tracking software (Trackpy [28]) to locate particle centers with an accuracy of ~ 30 nm in the horizontal direction. Likewise, the images are used to trace the interface position using OpenCV [29]. We finally verify the enhanced emulsion stability by comparing the stability of a particle-laden binary liquid emulsion with that of the pure binary liquid without particles. The particles are added at a volume fraction of 0.2 %, and the resulting mixtures with and without particles are sealed in glass vials and placed in a water bath for direct observation of the emulsion stability.

## 3. Results and discussions

### 3.1. Detachment of particles from the interface

When heating the homogeneous liquid mixture slowly from room temperature, we observe the onset of phase separation at a temperature of 33.6 °C, close to the value of $T_c$ reported in literature [30,31]. In the phase-separated region above $T_c$, extended interfaces between lutidine-rich and water-rich phases are observed as shown in Fig. 1C, where the bright upper half indicates the lutidine-rich, and the dark lower half the water-rich phase. The particles are located at the interface, visible as bright spots. At 10 K above $T_c$, the particles are situated centered at the interface: roughly one half of the particle sits in the water-rich phase and one half in the lutidine-rich phase (Fig. 1C). As we decrease the temperature towards $T_c$, the particles move slowly out of the interfaces into the water-rich phase. At $\Delta T = 4.4$ K, the particles have migrated out of the interface, as observed in Fig. 1G. At this and even lower temperatures, necking is observed as illustrated in Fig. 1B: particles that have moved into the water-rich phase are still connected to the lutidine-rich phase by capillary bridges, as observed in the inset of Fig. 1H (arrows). The particles pull the interface towards them, leading to apparent roughening of the interface. The necking leads to capillary interactions between the particles at the interface [32–34], which are much greater than $k_BT$, causing clustering of the particles at the interface. The main panel in Fig. 1H shows that at $\Delta T \sim 4.2$ K, many particles have left the interface, while some are still trapped at the interface. Moreover, the

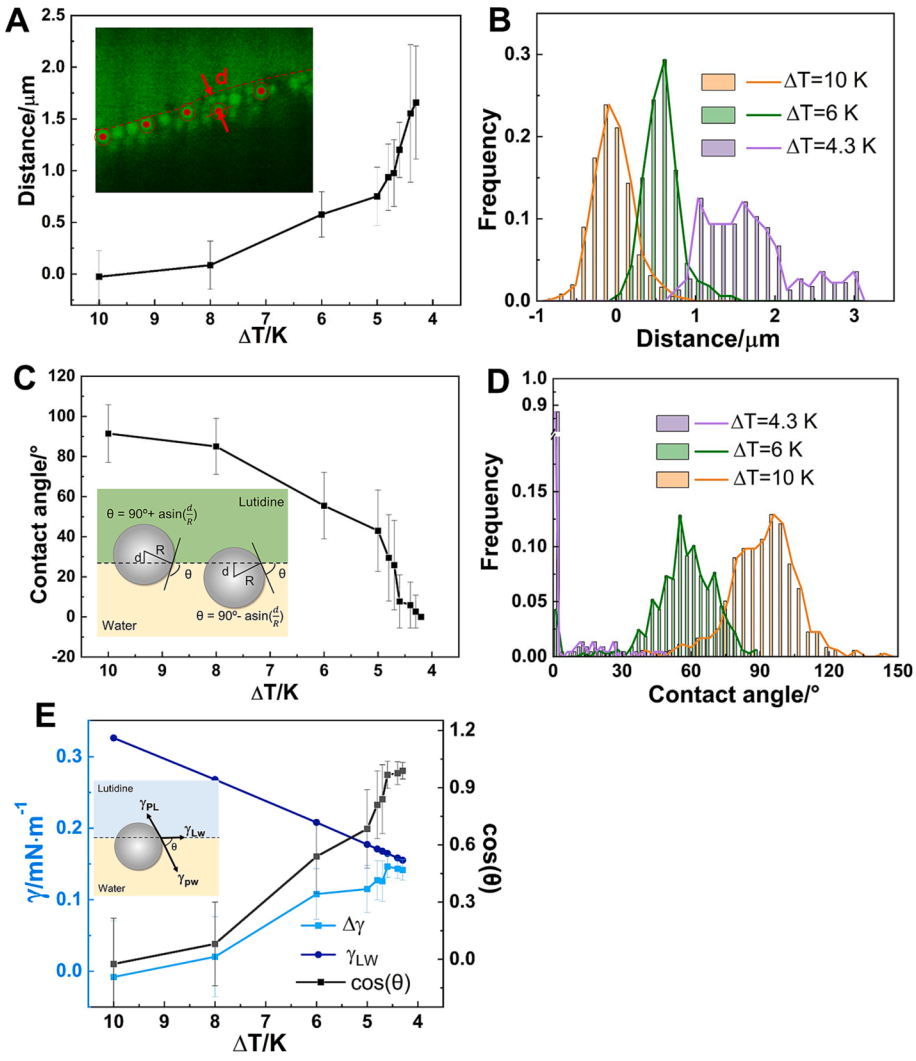


**Fig. 2.** Contact angle and interfacial tension. (A,B) Average distance of the particle centers from the interface as a function of temperature offset ΔT (A) and corresponding distribution of distances for three temperature offsets (B). Inset in (A) illustrates a few particle centers and determination of the particle - to - interface distance d. (C, D) Contact angle (C) and contact angle distribution (D) as determined from the particle-interface separations in A and B, see inset in (C) for illustration of the relationship. (E) Interfacial tension of the binary liquid $\gamma_{LW}$ from literature [31], cosine of the contact angle determined from the contact angle measurements in (C), and resulting interfacial tension difference $\Delta\gamma = \gamma_{PL} - \gamma_{PW}$ of particle-lutidine rich and particle-water rich phases computed using Young's equation.

particles remaining at the interface have formed aggregates because of the lateral capillary attraction, also multiple layers of particles can appear on the interface due to particle migration.

### 3.2. Contact angle ($\theta$)

To evaluate the detachment process quantitatively, we determine the distances $d$ of the particle centers from the interface, as illustrated in Fig. 2A, inset. The detachment process is clearly reflected in the growing separation of particle centers from the interface as shown in the main panel of Fig. 2A, exceeding the particle radius at approximately $\Delta T <$ 4.5 K. After that, particles are weakly connected to the interface by capillary bridges, as visible by the rugged interface in Fig. 1H, inset. This trend is reflected even more clearly in the distance distribution (Fig. 2B), which moves to the right and broadens at lower $\Delta T$, indicating the particle migration and eventual necking process.

This migration is driven by changes in the interfacial tension caused by changes in solvent composition, resulting in an overall change in particle contact angle. To obtain insight into this interplay, we determine the contact angle $\theta$ of the particle from its distance to the interface. As illustrated in Fig. 2C inset, both are related by $\theta = 90^\circ \pm \sin^{-1}(d/R)$, where $\theta = 90^\circ$ for particles centered at the interface, and $\theta = 0^\circ$ for particles with distance $d \geq R$ to the interface. The extracted average contact angle, shown in Fig. 2C, decreases with decreasing $\Delta T$ as the particle moves out of the interfaces. The corresponding contact angle distribution (Fig. 2D) shifts to the left, until it peaks at 0°, when the particles have migrated out of the interface and some are still loosely connected by capillary bridges. These results are robust (within error bars) with changes in particle volume fractions $\phi$ (see Supplementary Figure 1 for results at $\phi = 0.0004$ %). Changes in solvent composition, however, affect the particle detachment behavior: for off-critical solvent compositions, the surface tension is higher and remains finite upon approaching the phase separation line; for this system, we observe that particles remain attached until $\Delta T \sim 2$ K, and the contact angle versus $\Delta T$ dependence changes, see Supplementary Figure 2. Also changes in particle material are expected to affect the temperature-dependent particle detachment behavior, and preliminary measurements on more complex particles shown in Supplementary Figure 3 seem to confirm this.

The contact angle is the crucial quantity determining the particles' positions at the interface; to understand its evolution, we look at the interfacial tensions of the three involved phases, lutidine-rich (L) and

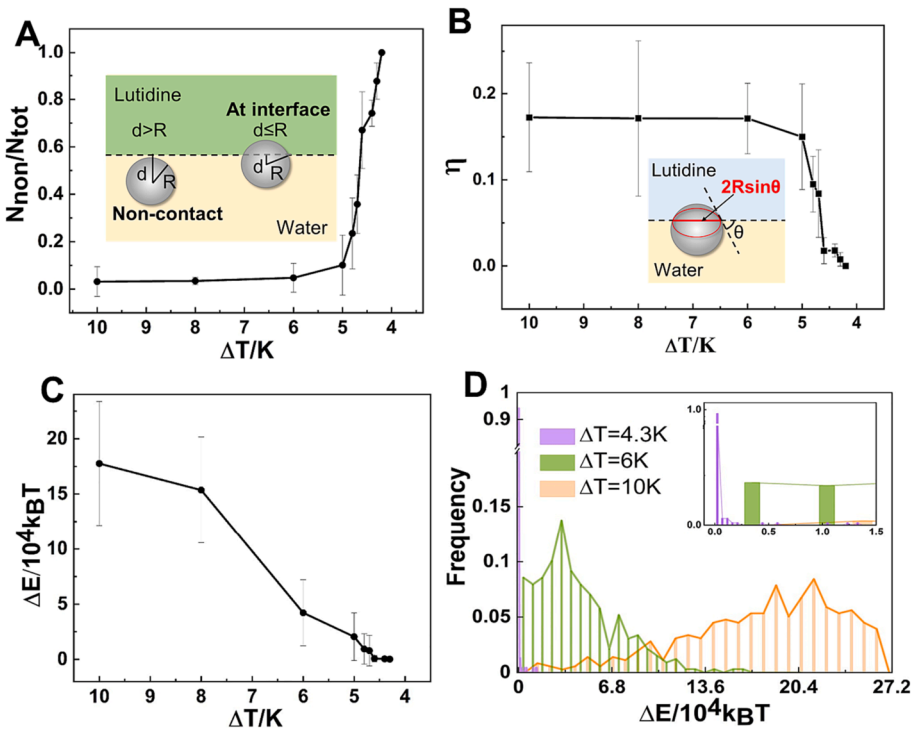


**Fig. 3. Surface coverage and interfacial energy.** (A) Fraction of particles detached from the interface as a function of temperature offset $\Delta T$. (B) Interface area fraction $\eta$ covered by particles at the interface as a function of $\Delta T$. (C) Detachment energy of a particle as a function of $\Delta T$. (D) Distribution of detachment energies for three temperature offsets.

water-rich (W) liquid phases, and the solid particle (P). The balance of the corresponding interfacial tensions $\gamma_{LW}$, $\gamma_{PL}$, and $\gamma_{PW}$, determines the contact angle according to Young's equation [35]:

$$\gamma_{PL} - \gamma_{PW} = \gamma_{LW} cos(\theta), \tag{2}$$

as illustrated in Fig. 2E inset. To investigate the interplay of interfacial tensions in the particle detachment process, we use literature values of the temperature dependence of $\gamma_{LW}$ [31] together with the measured contact angle to determine the surface tension difference $\Delta\gamma$=($\gamma_{PL}$ - $\gamma_{PW}$) of the particles with the lutidine and water-rich phases. Fig. 2E shows that at large $\Delta T$, far above $T_c$, the solvent interfacial tension $\gamma_{LW}$ dominates, pulling the particles to the interface, thus minimizing the interface area between the two liquid phases. As the temperature decreases, $\gamma_{LW}$ decreases and $\Delta\gamma$ increases until they approach each other. At this point, there is no energetic advantage any more for the particle to sit at the interface and the particles start detaching. Interestingly, the microscope images in Fig. 1G, H suggest that in this case, liquid bridging still leads to some degree of attachment and clustering, keeping some of the particles close to the interface.

### 3.3. Detachment energy

The ceasing energetic advantage is reflected in a diminishing particle coverage at the interface. To quantify this, we monitor the number of particles attached to the interface as a function of temperature as shown in Fig. 3A. Far above $T_c$, essentially all particles sit at the interface to lower the interfacial energy [36]. This situation persists until the energy cost $\gamma_{LW}$ becomes of the order of the energy gain $\Delta\gamma$ of the particle to be in the water-rich opposed to the lutidine-rich phase: the particles start to desorb from the interface, reflected in a rapid drop of the number of absorbed particles. Even before particles desorb, their gradual shift into the water-rich phase lowers their effective surface coverage: the effective interface area covered by a particle is $\pi(Rsin\theta_i)^2$, as determined by its contact angle, $\theta_i$. Therefore, the effective fraction of the surface occupied by all particles is:

$$\eta = \sum_i \pi(Rsin\theta_i)^2 \Big/ \Delta A \ , \tag{3}$$

where we sum over all particles in the field of view, and divide by the total imaged interface area $\Delta A$, which we estimate from the length of the interface in the image and the image's depth of focus. The latter can be estimated by the width of the point spread function of the confocal imaging system to be ~ 3.3 μm for our imaging conditions. The occupied surface fraction $\eta$, shown in Fig. 3B, decreases sharply for $\Delta T < 5$ K, and vanishes as $\Delta T$ approaches 4.3 K. The decrease of $\eta$ reflects both the decreasing contact angle of the particles, reducing the effective interface area per particle, as well as the desorption of the particles from the interface (Fig. 3A). The starting value $\eta \sim 0.17$ is set by the particle concentration in the suspension, which was chosen to be relatively low to observe the particle detachment process most clearly. Higher concentrations would be beneficial for stabilization of the emulsion, but hinder the microscopic imaging and make quantitative analysis of the images difficult.

We can finally use the measured contact angle and liquid interface tension $\gamma_{LW}$ from literature to compute the detachment energy $\Delta E$ according to Eq. (1). Results are shown in Fig. 3C. Far above $T_c$, the detachment energy is several orders of magnitude larger than the thermal energy, indicating the particle is firmly attached to the interface. As the temperature decreases and approaches $\Delta T = 4.3$ K, the contact angle vanishes and $\Delta E$ ceases, and the particles start desorbing from the interface. The distribution of $\Delta E$ shown in Fig. 3D reflect this trend in more detail. For large $\Delta T$, the entire distribution is $\gg k_B T$, keeping the particles anchored firmly at the interface, while for $\Delta T \leq 6$ K, the distribution has shifted to the left, leading to partial particle desorption from the interface, as reflected in the decrease of the surface coverage in Fig. 3B. This trend continues until at $\Delta T = 4.3$ K, $\Delta E$ becomes of the order of the thermal energy, and the particles detach from the interface. The growing interfacial tension between the particles and the lutidine-rich phase with respect to that of the particle and water-rich phase ($\Delta\gamma$ plotted in Fig. 2E) shows that the particles exhibit an increasing affinity

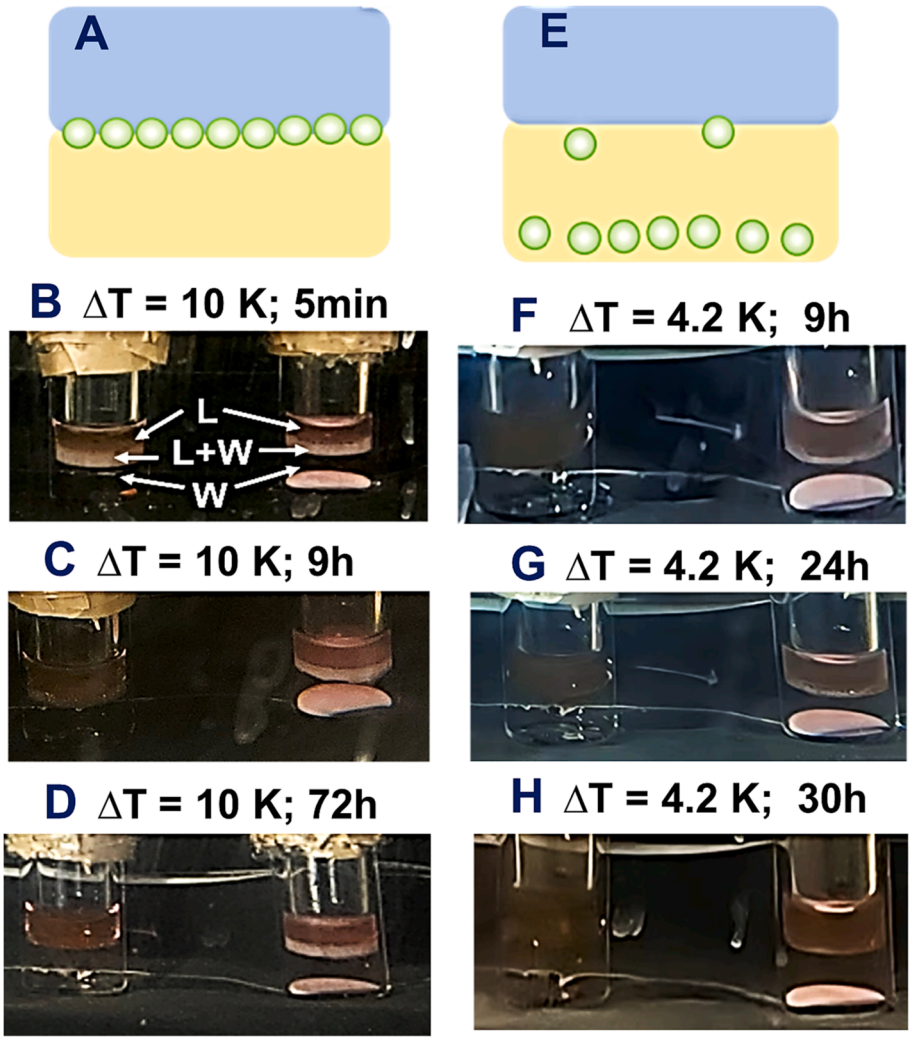


**Fig. 4. Emulsion stability.** Stability of the binary-liquid emulsion with and without colloidal particles at ΔT = 10 K (left) and ΔT = 4.2 K (right). (A, E) Illustration of the microscopic particle configurations at these two temperatures. (B-D) Photographs of the samples at $\Delta T$ = 10 K, 5 min (B), 9 h (C) and 72 h (D) after phase separation of the binary liquid. The sample with particles is shown on the right, and the sample without particles (reference) on the left. Arrows indicate lutidine-rich phase (L), water-rich phase (W), and emulsion layer (L + W). In addition, a layer of sedimented particles (pink) is observed at the bottom of the particle-containing sample (right). The Pickering emulsion persists even after 72 h, while the reference, the emulsion without particles, is barely stable. (F, G, H) Photographs of the same vials as in (B) - (D) at $\Delta T$ = 4.2 K, 9 h (F), 24 h (G) and 30 h (H) after phase separation. At this temperature, even the Pickering emulsion is barely stable, in agreement with the microscopic observation of particle detachment in Figs. 1 to 3. (For interpretation of the references to colour in this figure legend, the reader is referred to the web version of this article.)

to the more polar water-rich phase at lower temperatures.

### 3.4. Emulsion stability

To relate the microscopic adsorption behavior of particles to the macroscopic emulsion stability, we prepare large samples in vials and follow their stability over several days. We prepare two samples, one with the binary liquid alone, serving as reference, and the other containing particles with a volume fraction of 0.2 % in the binary liquid, sufficiently high to obtain good emulsion stability. The samples are put in glass vials for direct inspection. They are heated in a water bath to $\Delta T$ = 10 K, where they phase separate and form an emulsion. We then observe the emulsion stability over several days at two temperatures: at (i) $\Delta T$ = 10 K, and (ii) $\Delta T$ = 4.2 K, where particle detachment has been observed by microscopy. Images of the reference sample (left) and the sample with particles (right) at $\Delta T$ = 10 °C, immediately after phase separation are shown in Fig. 4B. The emulsified lutidine-water phase (L + W) is sandwiched between the lutidine-rich (L) phase at the top and the water-rich (W) phase at the bottom. Both samples show roughly equal amount of emulsified phase. In addition, a layer of sedimented particles is visible at the bottom of the vial on the right (d). After 9 h, the reference sample (left) shows almost no emulsion anymore: the upper (lutidine-rich) phase is directly on top of water-rich phase, separated by a nearly clear interface. In contrast, the sample with particles (right), still shows the emulsion layer between the upper and lower phases. For this sample, most of the emulsified layer still exists after 72 h, while in the reference sample, the emulsion layer has completely disappeared. This indicates that with particles, the emulsion is stable even after 3 days, which we associate with the presence of particles at the interface as observed by microscopy. This is further confirmed when we repeat the experiment at a lower temperature, $\Delta T$ = 4.2 K. Here, even with particles, the emulsion is already barely visible after 9 h, and has completely disappeared after 30 h. We associate this emulsion instability with the microscopic detachment of the particles from the interface, as observed in Figs. 2 and 3, causing droplets to coalescence to reduce their interface energy, which confirms that particles have to be anchored at the interface to stabilize the system. A similar conclusion was drawn by Matsubara *et al.*, who observed de-emulsification when the wetting

properties of the particles changed [24].

## 4. Conclusions

Using the temperature dependence of the interfacial tension of a phase-separated binary solvent, we have investigated the microscopic desorption behavior of particles in a Pickering emulsion. The binary solvent system allows us to continuously change the interfacial tension of the two liquid phases, thus enabling detailed observation of the particle detachment process. We observe particle detachment at finite interfacial tension of the liquids significantly above $T_c$, when the interfacial tension of the liquid phases equals the interfacial tension difference of the particle with respect to the two liquid phases. At this point, the energetic advantage of the particles to sit at the interface vanishes. The detailed microscopic imaging shows that necking between the particles at the liquid interface leads to clustering of particles at the interface before their detachment. The concomitant macroscopic observations show that the particle detachment leads to a loss of the stability of the emulsion. These results show that the macroscopic emulsion stability is related to the microscopic detachment of the particles from the droplet interfaces, governed by the interplay of interface tensions between the liquid–liquid and liquid–solid phases, setting the particles contact angle at the interface. The results highlight the microscopic interplay of surface tensions governing particle detachment, and their effect on the macroscopic stability of Pickering emulsions important for applications in foods and cosmetics. In these applications, the emulsion stability critically affects the shelf life of the product, therefore its microscopic understanding is crucially important. The observed reversibility of the particle attachment suggests that reversible emulsion stabilization/de-stabilization can be formulated, which can be relevant for the end-life of the product or for pharmaceutical encapsulation. Future studies can include systematic variation of the particle material in terms of its affinity to the liquid phases, as well as the use of more complex particles such as patchy particles having hydrophobic or hydrophilic patches, modelling much more complex adsorbed species such as proteins, which are used in food Pickering emulsions.

## CRediT authorship contribution statement

**Fu Zhen Zhou:** Data curation, Formal analysis, Investigation, Methodology, Software, Validation, Visualization, Writing – original draft. **Piet J.M. Swinkels:** Investigation, Software. **Shou Wei Yin:** Funding acquisition, Supervision. **Krassimir P. Velikov:** Conceptualization, Supervision, Writing – review & editing. **Peter Schall:** Conceptualization, Funding acquisition, Project administration, Supervision, Writing – review & editing.

## Declaration of competing interest

The authors declare that they have no known competing financial interests or personal relationships that could have appeared to influence the work reported in this paper.

## Data availability

Data will be made available on request.

## Acknowledgments

The authors would also like to thank the China Scholarship Council (CSC) research program for providing funding for F. Z. Zhou.

## Appendix A. Supplementary data

Supplementary data to this article can be found online at https://doi.org/10.1016/j.jcis.2024.02.070.

## References

[1] S.N. Kale, S.L. Deore, Emulsion micro emulsion and nano emulsion: a review, Systematic Reviews in Pharmacy 8 (1) (2017) 39.
[2] L. Rekvig, M. Kranenburg, B. Hafskjold, B. Smit, Effect of surfactant structure on interfacial properties, Europhys. Lett. 63 (6) (2003) 902.
[3] S.U. Pickering, Cxcvi.—emulsions, J. Chem. Soc. Trans. 91 (1907) 2001–2021.
[4] B.P. Binks, Particles as surfactants—similarities and differences, Curr. Opin. Colloid Interface Sci. 7 (1) (2002) 21–41.
[5] J. Wu, G.-H. Ma, Recent studies of pickering emulsions: particles make the difference, Small 12 (34) (2016) 4633–4648.
[6] L.E. Low, S.P. Siva, Y.K. Ho, E.S. Chan, B.T. Tey, Recent advances of characterization techniques for the formation, physical properties and stability of Pickering emulsion, Adv. Colloid Interface Sci. 277 (2020) 102117.
[7] A.W. Folkmann, A. Putnam, C.F. Lee, G. Seydoux, Regulation of biomolecular condensates by interfacial protein clusters, Science 373 (6560) (2021) 1218–1224.
[8] E. Guzmán, F. Ortega, R.G. Rubio, Pickering emulsions: a novel tool for cosmetic formulators, Cosmetics 9 (4) (2022) 68.
[9] Y. Yang, Z. Fang, X. Chen, W. Zhang, Y. Xie, Y. Chen, Z. Liu, W. Yuan, An overview of Pickering emulsions: solid-particle materials, classification, morphology, and applications, Front. Pharmacol. 8 (2017) 287.
[10] H. Jiang, Y. Sheng, T. Ngai, Pickering emulsions: Versatility of colloidal particles and recent applications, Curr. Opin. Colloid Interface Sci. 49 (2020) 1–15.
[11] S. Lam, K.P. Velikov, O.D. Velev, Pickering stabilization of foams and emulsions with particles of biological origin, Curr. Opin. Colloid Interface Sci. 19 (5) (2014) 490–500.
[12] H. Dai, J. Wu, H. Zhang, Y. Chen, L. Ma, H. Huang, Y. Huang, Y. Zhang, Recent advances on cellulose nanocrystals for Pickering emulsions: development and challenge, Trends Food Sci. Technol. 102 (2020) 16–29.
[13] E.M. Nomena, C. Remijn, F. Rogier, M. van der Vaart, P. Voudouris, K.P. Velikov, Unravelling the mechanism of stabilization and microstructure of oil-in-water emulsions by native cellulose microfibrils in primary plant cells dispersions, ACS Applied Bio Materials 1 (5) (2018) 1440–1447.
[14] L. Chen, F. Ao, X. Ge, W. Shen, Food-grade pickering emulsions: preparation, stabilization and applications, Molecules 25 (14) (2020) 3202.
[15] C.C. Berton-Carabin, K. Schroën, Pickering emulsions for food applications: background, trends, and challenges, Annu. Rev. Food Sci. Technol. 6 (2015) 263–297.
[16] X. Yan, C. Ma, F. Cui, D.J. McClements, X. Liu, F. Liu, Protein-stabilized pickering emulsions: formation, stability, properties, and applications in foods, Trends Food Sci. Technol. 103 (2020) 293–303.
[17] M. Rutkevičius, S. Allred, O.D. Velev, K.P. Velikov, Stabilization of oil continuous emulsions with colloidal particles from water-insoluble plant proteins, Food Hydrocoll. 82 (2018) 89–95.
[18] F. Zhou, X. Yu, D. Luo, X. Yang, S. Yin, Pickering water in oil emulsions prepared from biocompatible gliadin/ethyl cellulose complex particles, Food Hydrocoll. 134 (2023) 108050.
[19] D.J. French, A.T. Brown, A.B. Schofield, J. Fowler, P. Taylor, P.S. Clegg, The secret life of Pickering emulsions: particle exchange revealed using two colours of particle, Sci. Rep. 6 (1) (2016) 31401.
[20] Y. Chai, J. Hasnain, K. Bahl, M. Wong, D. Li, P. Geissler, P.Y. Kim, Y. Jiang, P. Gu, S. Li, D. Lei, B.A. Helms, T.P. Russell, P.D. Ashby, Direct observation of nanoparticle-surfactant assembly and jamming at the water-oil interface, Sci. Adv. 6 (48) (2020) eabb8675.
[21] M. Reeves, K. Stratford, J.H. Thijssen, Quantitative morphological characterization of bicontinuous Pickering emulsions via interfacial curvatures, Soft Matter 12 (18) (2016) 4082–4092.
[22] E. Sanz, K.A. White, P.S. Clegg, M.E. Cates, Colloidal gels assembled via a temporary interfacial scaffold, Phys. Rev. Lett. 103 (25) (2009) 255502.
[23] E.M. Herzig, K.A. White, A.B. Schofield, W.C.K. Poon, P.S. Clegg, Bicontinuous emulsions stabilized solely by colloidal particles, Nat. Mater. 6 (12) (2007) 966–971.
[24] H. Matsubara, K. Chiguchi, B.M. Law, Pickering emulsion transitions in 2,6-lutidine plus water critical liquid mixtures, Langmuir 36 (42) (2020) 12601–12606.
[25] K.A. White, A.B. Schofield, P. Wormald, J.W. Tavacoli, B.P. Binks, P.S. Clegg, Inversion of particle-stabilized emulsions of partially miscible liquids by mild drying of modified silica particles, J. Colloid Interface Sci. 359 (1) (2011) 126–135.
[26] T.E. Kodger, R.E. Guerra, J. Sprakel, Precise colloids with tunable interactions for confocal microscopy, Sci. Rep. 5 (1) (2015) 14635.
[27] P.J.M. Swinkels, S.G. Stuij, Z. Gong, H. Jonas, N. Ruffino, B. Linden, Revealing pseudorotation and ring-opening reactions in colloidal organic molecules, Nat. Commun. 12 (1) (2021) 2810.
[28] D.C. Allan, K. Thomas, N. van der Wel, C. Trackpy. community, Trackpy v0.3.0. Zenodo http://zenodo.org/record/34028. 2014.
[29] P. Joshi, OpenCV with Python by example, Packt Publishing Ltd:, 2015.
[30] A. Mukhopadhyay, Curved colloidal crystals of discoids at near-critical liquid–liquid interface, Soft Matter 17 (29) (2021) 6942–6951.
[31] C.A. Grattoni, R.A. Dawe, C.Y. Seah, J.D. Gray, Lower critical solution coexistence curve and physical properties (density, viscosity, surface tension, and interfacial tension) of 2,6-lutidine + water, J. Chem. Eng. Data 38 (4) (1993) 516–519.
[32] T. Brugarolas, B.J. Park, M.H. Lee, D. Lee, Generation of amphiphilic janus bubbles and their behavior at an air-water interface, Adv. Funct. Mater. 21 (20) (2011) 3924–3931.
[33] D. Stamou, C. Duschl, D. Johannsmann, Long-range attraction between colloidal spheres at the air-water interface: the consequence of an irregular meniscus, Phys. Rev. E 62 (4) (2000) 5263–5272.

[34] P.A. Kralchevsky, N.D. Denkov, K.D. Danov, Particles with an undulated contact line at a fluid interface: interaction between capillary quadrupoles and rheology of particulate monolayers, Langmuir 17 (24) (2001) 7694–7705.
[35] B.P. Binks, J.H. Clint, Solid wettability from surface energy components: relevance to pickering emulsions, Langmuir 18 (4) (2002) 1270–1273.
[36] E. Guzmán, F. Ortega, R.G. Rubio, Forces controlling the assembly of particles at fluid interfaces, Langmuir 38 (44) (2022) 13313–13321.